

G2C2 I: Homogeneous photometry for Galactic Globular Clusters in SDSS passbands

Joachim Vanderbeke^{1,2*}, Michael J. West^{2,3}, Roberto De Propris⁴, Eric W. Peng^{5,6}, John P. Blakeslee^{8,9}, Andrés Jordán⁷, Patrick Côté⁸, Michael Gregg^{10,11}, Laura Ferrarese⁸, Marianne Takamiya¹², Maarten Baes¹

¹ *Sterrenkundig Observatorium, Universiteit Gent, Krijgslaan 281 S9, B-9000 Gent, Belgium*

² *European Southern Observatory, Alonso de Córdova 3107, Vitacura, Santiago, Chile*

³ *Maria Mitchell Observatory, 4 Vestal Street, Nantucket, MA 02554, USA*

⁴ *Finnish Centre for Astronomy with ESO (FINCA), University of Turku, Väisäläntie 20, FI-21500 Piikkiö, Finland*

⁵ *Department of Astronomy, Peking University, Beijing 100871, China*

⁶ *Kavli Institute for Astronomy and Astrophysics, Beijing 100871, China*

⁷ *Instituto de Astrofísica, Facultad de Física, Pontificia Universidad Católica de Chile, Av. Vicuña Mackenna 4860, 7820436 Macul, Santiago, Chile*

⁸ *Herzberg Institute of Astrophysics, National Research Council, Victoria, BC V9E2E7, Canada*

⁹ *Department of Physics and Astronomy, Washington State University, 1245 Webster Hall, Pullman, WA 99163-2814, USA*

¹⁰ *Department of Physics, University of California, Davis, CA 956160, USA*

¹¹ *Institute for Geophysics and Planetary Physics, Lawrence Livermore National Laboratory, L-413, Livermore, CA 94550, USA*

¹² *Physics and Astronomy Department, University of Hawaii Hilo, Hilo, HI 96720, USA*

Accepted. Received

ABSTRACT

We present g' and z' aperture photometry for 96 Galactic Globular Clusters, making this the largest homogeneous catalog of photometry for these objects in the SDSS filter system. For a subset of 56 clusters we also provide photometry in r' and i' . We carry out comparisons with previous photometry as well as with the SDSS dataset. The data will be useful for a series of applications in Galactic and extragalactic astrophysics. Future papers will analyse the colour-metallicity relation, colour-magnitude diagrams, and structural parameters. The compilation of results based on this dataset will be collected in the Galactic Globular Cluster Catalog (G2C2).

Key words: Galactic Globular Clusters

1 INTRODUCTION

Globular clusters (hereafter GCs) formed during the earliest episodes of star formation in galaxies. They are found in all but the smallest dwarf galaxies, with massive galaxies hosting systems of hundreds or thousands of clusters. The properties of globular clusters appear to be very homogeneous from one galaxy to the other (in terms of colour, luminosity distribution, etc.) and this implies that the formation of these objects has been intimately related to the assembly of their parent galaxies (e.g., Harris 1991). Globular clusters are living fossils of the Universe at high redshift (their mass is similar to the Jeans mass at the epoch of recombination) and therefore give a snapshot of conditions as prevailed at early epochs (see West et al. 2004; Brodie & Strader 2006 for reviews). The integrated properties of globular clusters therefore provide us with information on the earliest stages of galaxy formation; the high intrinsic luminosities of clusters means that they can be studied in de-

tail well beyond the Local Group, while the bright end of the globular cluster luminosity function has been detected around a $z \sim 0.2$ elliptical galaxy (Alamo-Martínez et al. 2013).

Most work in both Galactic and extragalactic GCs is still based on the older photometric systems (such as Johnson-Cousins, Washington, etc.). Several authors have remarked on the lack of calibrating studies of globular clusters in the SDSS system (Jordán et al. 2005; Sinnott et al. 2010; Peacock et al. 2011; Vickers et al. 2012); as most such objects are in the South, the vast majority of Galactic GCs have not been imaged by the SDSS survey. The latest edition of the Harris (1996) compilation (2010 edition, this is the version we refer to in the remainder of the paper) lists $UBVRI$ colours for about half of the 150 Galactic GCs. Nevertheless, this photometry is inhomogeneous, as it is taken from different papers, using different methods and instruments (including photomultipliers, photographic plates and modern CCDs).

The Sloan Digital Sky Survey (SDSS – York et al. 2000) has now imaged over a quarter of the Northern sky (about 14500 square degrees) in five passbands. Together with upcoming imaging sur-

* E-mail: Joachimvanderbeke@gmail.com

Table 1. The instrumental set-up.

| | |
|----------------|------------------------------------|
| Telescope | CTIO 0.9m |
| Dates | 2003 May - 2012 March |
| Filter set | $g'r'i'z'$ |
| Spatial scale | $0.396'' \text{ pixel}^{-1}$ |
| Field Size | $13.6' \times 13.6'$ |
| Gain | $3.0 \text{ e}^- \text{ ADU}^{-1}$ |
| Read-out noise | 5 e^- |
| Detector | 2048×2046 Tek2K CCD |

veys in the South, SDSS will completely replace the older Schmidt plate atlases of the sky, and at the same time provide a standardized system of photometry in the optical for astrophysics (theoretically, with calibrators in every field). With this motivation, our team embarked on the Galactic Globular Cluster Catalog (G2C2) project, with an ultimate goal of collecting reliable photometry using the SDSS filter system for a large sample of Galactic GCs. In this first paper, we present g' and z' magnitudes for about two-thirds of the Galactic GCs and r' and i' magnitudes for about one-third of all Galactic GCs. Future work will discuss the colour-metallicity relation (see the companion Paper II – Vanderbeke et al. 2013, in press), the colour-magnitude diagrams of these clusters, their spectral energy distributions over 2 decades in wavelength, and the structural parameters of GCs using King models.

Here we discuss the buildup of the photometric database: imaging of 96 Galactic clusters in at least 2 SDSS bands (as well as 2 more for a subset of 56 objects). We describe our observations and basic data reduction: we give details about the samples, determination of cluster centres, aperture photometry, estimation of the sky level, removal of outliers, photometric errors and correction for extinction. To assess the quality of our data we compare these with previous work and carry out a similar analysis on globular clusters in common with the SDSS footprint. This paper is organized as follows. Section 2 presents the observations and the basic data reduction. We present the integrated photometry and colours for the Galactic GCs in Section 3. We summarize the results in Section 4.

2 OBSERVATIONS AND DATA REDUCTION

2.1 CTIO

We selected Galactic GCs from the latest versions of the Harris (1996) catalog, which includes about 150 GCs. Observations were carried out between 2003 May 10 and 2012 June 9 using the CTIO 0.9 m and 1 m telescopes with the USNO $g'r'i'z'$ filter set. Because the Galactic bulge and hence the bulk of the Galactic GCs are best observable during the Chilean winter, cirrus and bad weather were a real issue during the observing runs: many nights were totally lost due to clouds or strong winds, while other nights were disturbed by cirrus and were not photometric.

For the results in this paper, we reduced 13 nights of observations. Several clusters were observed multiple times and it became clear that only 4 nights (all of which used the 0.9 m telescope, with an instrumental set-up as shown in Table 1) could be considered (largely) photometric. During these nights, we collected g' and z' observations for 81 GCs, about half of which we also observed using r' and i' filters.

For the vast majority of the clusters, we have 60 s exposures in g' and z' taken in June 2004. During the run performed on 2003 May 10 short (between 5 and 30 s) and long (270 s in g' , 410 s

in z') exposures were obtained. Both shorter and longer exposures were used separately to determine magnitudes. Some of the clusters have very bright stars close to their centres. These very bright stars saturated the CCD even for the short exposures. For these clusters (NGC 6397, 47 Tuc, NGC 6121) we obtained additional 1 s exposures. The observations discussed in this paper were performed between 2003, May 10 and 2005, September 26 under seeing conditions varying between $1''$ and $\sim 2''$.

The basic data reduction was performed via a dedicated IDL pipeline developed by our team. The procedure largely follows conventional CCD reduction processes. The bias level was estimated separately for each quadrant of the CCD, by computing the median of the corresponding bias section, which was then subtracted for each quadrant. The frames were then flat-fielded by the median of the twilight flats taken each night and corrected for bad columns. To identify and robustly remove cosmic rays, we used the L.A. Cosmic (imaging version) method (van Dokkum 2001).

One additional complication was the incorrect information in the fits headers of the clusters observed from 2005 onwards. John Subasavage (private communication) confirmed that, since the TCS upgrade in early 2005, the header values (including RA, DEC, airmass and epoch) are not correct. Based on the coordinates obtained from Harris (1996) and the header values (date and time of observation), we computed automatically the airmasses for the observations taken after 2005. Comparison with observation log sheets showed excellent agreement.

During the course of each observing night a minimum of several dozen standard stars, selected from Smith et al. (2002), were observed at different airmasses. Photometric calibration (i.e., determination of zeropoints, colour terms and atmospheric extinction values, as well as removal of other instrumental signatures) was carried out as in Patat & Carraro (2001). Foreground (galactic) extinction was estimated for each position using the most recent values from the recalibration of Schlafly & Finkbeiner (2011).

2.2 SDSS Data Release 9

We also considered a sample of 21 northern hemisphere clusters from the ninth data release of SDSS (Ahn et al. 2012), 6 of which have also been observed by us with the CTIO 0.9m telescope. However, NGC 6838 and NGC 6254 were only partly covered by SDSS and were not included in this study, as our procedure (see below) requires us to cover at least the half-light radius in each object. Bright foreground stars outshine GLIMPSE01, Ko 1 and Ko 2. We do not consider these clusters further.

For some other clusters, several SDSS stripes needed to be assembled into mosaics using Montage¹, although this may lead to issues with variable sky levels. Although SDSS data have the considerable advantage of being photometrically homogeneous and uniform, the 53.9 s standard exposure in SDSS saturates bright red giant branch (RGB) stars in some GCs, an effect which becomes clear when comparing the colour magnitude diagrams and which is further discussed in Section 3.6. Note that the 'SDSS' filters at the APO 2.5m telescope (and the CTIO 0.9m) have significantly different effective central wavelengths from the calibrating filters at the USNO 1m telescope, where the $u'g'r'i'z'$ photometric system was defined (Fukugita et al. 1996) and extended with secondary standards by Smith et al. (2000, 2002). The conversion between the

¹ <http://montage.ipac.caltech.edu/>

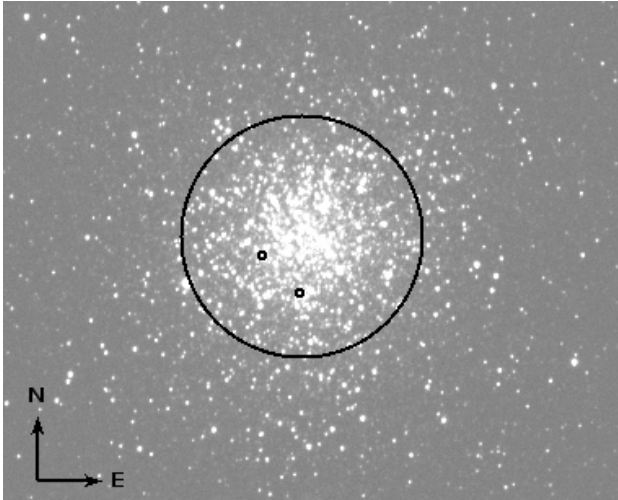


Figure 1. g' -band observation of NGC 5986. The half-light radius is indicated with the big circle, while the small circles indicate two stars that are likely non-members (contaminants) as selected from their position in the cluster colour-magnitude diagram.

$u'g'r'i'z'$ and $ugriz$ system is given on the SDSS website². These result in negligible changes to the GC colours when compared to the magnitude uncertainties.

For NGC 6341 and NGC 5904 the saturation of the SDSS chip was so severe that almost the entire RGB is brighter than the saturation limit of the CCD. It was nearly impossible to select non-saturated stars to construct the PSF for the CMDs, which are indispensable in the reduction process (see Section 3.3). We decided to discard these clusters from the sample. Nevertheless, good quality data for NGC 6341 is highly desirable, as this GC is one of the most metal-poor GCs of the Milky Way.

3 INTEGRATED PHOTOMETRY OF GLOBULAR CLUSTERS

Galactic GCs are generally too large on the sky to be completely included within a single CCD frame (see Figure 1 for an example from our own data). Although we experimented with fitting King models to the surface brightness profiles of the GCs to measure total magnitudes (we discuss this in a subsequent paper), we ultimately chose to derive aperture magnitudes within the clusters' half-light radii (e.g., Peng et al. 2006) to determine integrated colours. As long as the clusters show no strong colour gradients in their outskirts, the integrated colours we present here should be suitable proxies for studies of extragalactic systems as well.

We measured the aperture magnitude within the half-light radius r_h obtained from Harris (1996) where the original values are drawn largely from Trager et al. (1993, 1995) and McLaughlin & van der Marel (2005). As the largest r_h is 5 arcminutes, it does not completely fill the CCD field-of-view and therefore enables us to determine magnitudes for all clusters in a homogeneous manner (as in Peng et al. 2006). To obtain a total magnitude for the clusters, we would need imaging reaching well beyond the tidal radius. However, the largest tidal radius for the Galactic GCs is 53.8 arcminutes, much bigger than our field-of-view. As long as colour

gradients in the cluster outskirts are not very strong, the integrated colours determined within the $1/2$ light radius aperture should be representative of the total colours. To illustrate this for a cluster with a tidal radius r_t which fits the CTIO 0.9m telescope field-of-view, we compared the $g' - z'$ colour based on r_h and r_t apertures for NGC 5694. After correcting for contaminants (as will be described in Section 3.3) the colour difference between r_h and r_t apertures is 0.002 mag for this cluster, which is negligible compared to the magnitude uncertainties.

NGC 6287 and NGC 6553 are other clusters with a tidal radius small enough to be entirely covered by the CTIO field-of-view. However, NGC 6287 was not centred properly on the chip and was not entirely covered as a consequence. The observations of NGC 6553 included some saturated stars within the tidal radius, which is complicating the cleaning of the contaminants and impeding a proper comparison of the colours within the half-light and tidal radii.

Our first step will be to determine the cluster centres for the apertures, followed by estimation of the sky values, removal of contaminants (foreground stars) and measurement of the total flux within the $1/2$ light radius. We then discuss extinction, photometric errors and compare our results with previous work and SDSS.

3.1 Cluster Centroids

Our first step is to determine an accurate cluster centroid for the apertures. For the CTIO data, we followed the method of Bellazzini (2007). We calculated the aperture fluxes in a grid of 25 points around the initial (visual) guess for the cluster centre: the size of the grid is 125 pixels or $60''$. The 'centre' position at which the aperture flux is maximal is adopted as the cluster centroid and used as the reference point for aperture photometry. This was performed separately for all frames, because of inconsistent coordinates in the headers. For the SDSS data, the coordinates listed in Harris (1996) were adopted together with the SDSS astrometric solution. The error in the photometry introduced by the uncertainty in the centre position is estimated in the following way (both for SDSS and CTIO data): magnitudes were computed for apertures centered at four grid points separated by 5% of the stated half-light radius; we calculated the magnitude difference between the aperture magnitudes centered on these positions and the 'true' centre we determined above. The median of this difference is used as the estimate of the uncertainty introduced by the centre determination and is summed in quadrature to the photometric and other errors to obtain the total magnitude error, assuming these errors are independent. The median contribution of the centre determination to the total magnitude uncertainty is 0.006 mag.

To provide a consistency check, we have compared the centroids in the g' -band to the more accurate central coordinates for each cluster as determined by Goldsbury et al. (2010) with HST/ACS data. The median difference between both centre determinations is $0.086 r_h$. Using $8.6\% r_h$ instead of $5\% r_h$ to determine the magnitude uncertainty due to the centre determination results in a median additional error of 0.004 mag, which is negligible when compared to the systematic error introduced in Section 3.5.

3.2 Sky values

Determination of the sky value proved challenging, as several clusters fill the 0.9m CCD and in most cases the images do not cover the clusters out to their tidal radius. We used MMM (Mean, Median,

² http://www.sdss.org/dr6/algorithms/jeg_photometric_eq_dr1.html

Mode), a routine available at the IDL astronomy library which was developed to estimate the sky background in a crowded field and was adapted from the DAOPHOT routine with the same name. The algorithm consists of several steps: it first computes the mean and standard deviation of the sky flux, which is used to eliminate outliers. MMM repeats the first step in up to 30 iterations recomputing the sky (eliminating outliers of the previous iteration). As a next step, MMM estimates the amount of stellar contamination by comparing the mean, mode and median of the remaining sky pixels. If the mean is less than the mode and the median, then the contamination is slight and the sky is estimated by the mean. If the mean is larger, indicating severe contamination (as the program assumes positive departures from the true sky value in crowded fields), then the true sky value is estimated by $3 \times \text{median} - 2 \times \text{mean}$. We applied the MMM method to the four corners of each frame in a 100 by 100 pixel area, summing up about 40000 pixels (as some pixels will be identified as outliers by MMM and will not contribute to the sky determination). We regard these regions as the best approximation for the sky value.

The SDSS pipeline processing the data includes the sky subtraction, hence the sky value for these frames is always about zero. For consistency, we did determine the sky value running MMM on the entire mosaic.

Photometric uncertainties introduced when determining the sky level are further discussed in Section 3.5.

3.3 Removing foreground stars

Contamination from foreground bulge or disk stars can be severe at low Galactic latitudes and a number of methods have been proposed to tackle this issue. In their study on the integrated 2MASS photometry of Galactic GCs, Cohen et al. (2007) considered stars brighter than the tip of the RGB by 1.5 mag as non-members and excluded them. However, it is difficult to use this approach close to the cluster centre (at least from the ground) because of crowding and the low spatial resolution of their (and our) data. Peng et al. (2006), for example, disregarded this correction.

Contaminating stars can be excluded in two ways: from their abnormal position in the cluster colour-magnitude diagram, which implies they are unlikely to be cluster members (e.g., if they lie well outside the cluster principal sequences), or from their measured proper motions, as cluster stars are unlikely to show detectable motions because of their great distances.

Although our data suffer from crowding, average seeing and poor spatial resolution, we were able to derive colour-magnitude diagrams to identify likely foreground stars and clean the aperture magnitudes. We carried out stellar photometry with DAOPHOT and ALLSTAR (Stetson 1987, 1994). As a first step, up to 50 isolated and bright stars were selected to model a point spread function (PSF), accounting for variation over the field by allowing quadratic variability. We used a PSF radius depending on the seeing: generally we used $4 \times \text{FWHM}$ but adopted a maximum of 15 pixels when the seeing was bad or the focus was mediocre. This aperture is large enough to remove the bulk of the contaminating star light but small enough to enable DAOPHOT to resolve the stars. DAOMATCH and DAOMASTER were used to crossmatch the different filters.

As a consequence of the low resolution of our data ($0.396''$ pixels and a seeing between $1''$ and $\sim 2''$), crowding does obviously affect the final CMDs, which are not complete, especially close to the centre. However, these cover large fields, extending well beyond the half-light radius where crowding is not as impor-

tant. A detailed analysis of these colour-magnitude diagrams will be presented in a forthcoming paper.

As an example, Fig. 2 shows the CMD for NGC 5986: open circles represent stars within the half-light radius, dots are stars from the entire field. This GC is located at a Galactic latitude of $b = 13.27^\circ$, so some contamination from the disk may be expected, and is visible as a blue plume of stars above the turnoff. As mentioned above we use the half-light radius to measure the aperture magnitudes of the cluster, so stars in this area (represented as open circles) that lie outside of the principal sequences are possible contaminants. For confirmation, we checked the bright outliers, indicated by red circles in Fig. 2, for proper motions in the USNO-B1.0 catalog (Monet et al. 2003) and the NOMAD catalog (Zacharias et al. 2005), although in many cases these are not fully conclusive (e.g., see McDonald et al. 2013 for a similar approach to the bright AGB stars in NGC 4372). Once we are convinced that the star is a true non-member, the star is cleaned from the cluster photometry by subtracting its flux, based on the DAOPHOT PSF magnitudes, from the flux in the cluster aperture. Removing these stars in NGC 5986 results in magnitude corrections of 0.06 (0.03, 0.02, 0.02) in g' (r' , i' , z' , respectively). It is interesting to note that the contaminating stars in NGC 5986 would not have been removed if we had followed Cohen et al. (2007) as they are fainter than the RGB tip.

The magnitude corrections for foreground contamination may sometimes be very large, especially in poor clusters: for Pal 10 these corrections are 1.33 (0.62, 0.39, 0.33) mag. in g' (r' , i' , z'). This yields a ~ 1 mag correction for contamination in $g' - z'$.

A caveat is that differential reddening may shift foreground stars into the cluster principal sequences: this can be significant for clusters at low galactic latitude, where extinction may be patchy (Alonso-García et al. 2012). While we discuss reddening related issues extensively in our study on the colour-metallicity relation, specifically as these affect the colour-magnitude relation, we believe that a few such outliers will not significantly affect the derived colours.

For the CTIO data, an extract of the magnitudes and the applied contamination corrections (denoted as $\text{CMD}_{g',r',i',z'}$) is listed in Table 2. The complete table is available in the electronic version of this paper. Magnitudes and contamination corrections for the SDSS data are given in Table 3.

3.4 Comparison with previous work

To test the reliability of our approach we compare our g' and z' magnitudes with Peng et al. (2006), which also uses the half-light radius. Moreover, their Galactic GC data was based on the observations performed on 2004 June 5 and 6, so there is a considerable overlap with our sample. We match our apertures to theirs (some measurements of structural parameters have since changed) and we use the $E(B - V)$ values from Harris (1996) which were used by Peng et al. (2006) and a Cardelli et al. (1989) reddening law instead of the reddening values from Schlafly & Finkbeiner (2011), for the sake of consistency in these comparisons. These are shown in Fig. 3: while there is no systematic offset, there are a couple of outliers, for which the magnitude difference with the earlier results (Peng et al. 2006) is larger than expected. It is unclear what the origin of the discrepancy is. In the next section, we discuss the origin of the photometric errors in more detail. It will become clear that the sky determination can strongly affect the final magnitudes, which we raise as possible cause for the variance when comparing to Peng et al. (2006). At least for NGC5927 the observing log of

Table 2. Extract of the GC $g'r'i'z'$ magnitudes and errors based on CTIO observations. $\text{CMD}_{g',r',i',z'}$ presents the magnitude corrections based on the CMDs. The complete table is available in the online version of the paper.

| ID | g' | $\sigma_{g'}$ | r' | $\sigma_{r'}$ | i' | $\sigma_{i'}$ | z' | $\sigma_{z'}$ | $\text{CMD}_{g'}$ | $\text{CMD}_{r'}$ | $\text{CMD}_{i'}$ | $\text{CMD}_{z'}$ |
|---------|--------|---------------|--------|---------------|--------|---------------|--------|---------------|-------------------|-------------------|-------------------|-------------------|
| NGC104 | 4.912 | 0.030 | ... | ... | ... | ... | 3.677 | 0.044 | 0.00 | ... | ... | 0.00 |
| NGC288 | 9.080 | 0.032 | 8.600 | 0.045 | 8.295 | 0.044 | 8.139 | 0.044 | 0.00 | 0.00 | 0.00 | 0.00 |
| NGC362 | 7.471 | 0.030 | 6.925 | 0.043 | 6.618 | 0.043 | 6.419 | 0.043 | 0.01 | 0.02 | 0.02 | 0.03 |
| NGC1261 | 9.474 | 0.031 | 8.995 | 0.045 | 8.744 | 0.045 | 8.582 | 0.045 | 0.03 | 0.05 | 0.06 | 0.06 |
| AM1 | 15.958 | 0.035 | 15.582 | 0.046 | 15.219 | 0.047 | 15.159 | 0.056 | 0.07 | 0.13 | 0.14 | 0.16 |
| NGC1851 | 8.280 | 0.031 | 7.703 | 0.044 | 7.413 | 0.044 | 7.194 | 0.044 | 0.03 | 0.04 | 0.05 | 0.05 |
| NGC1904 | 9.006 | 0.030 | 8.570 | 0.044 | 8.351 | 0.044 | 8.178 | 0.044 | 0.02 | 0.04 | 0.05 | 0.05 |
| NGC2298 | 9.650 | 0.039 | 9.287 | 0.050 | 9.036 | 0.052 | 8.865 | 0.054 | 0.06 | 0.10 | 0.10 | 0.10 |
| NGC2808 | 6.695 | 0.030 | 6.194 | 0.044 | 5.916 | 0.044 | 5.725 | 0.044 | 0.00 | 0.00 | 0.00 | 0.00 |

Table 3. GC $griz$ magnitudes and errors based on data from SDSS (Data Release 9). $\text{CMD}_{g,r,i,z}$ presents the magnitude corrections based on the CMDs.

| ID | g | σ_g | r | σ_r | i | σ_i | z | σ_z | CMD_g | CMD_r | CMD_i | CMD_z |
|----------|--------|------------|--------|------------|--------|------------|--------|------------|----------------|----------------|----------------|----------------|
| Whiting1 | 16.637 | 0.083 | 16.162 | 0.069 | 15.953 | 0.060 | 15.854 | 0.060 | 0.00 | 0.00 | 0.00 | 0.00 |
| Pal1 | 15.118 | 0.042 | 14.769 | 0.033 | 14.615 | 0.030 | 14.522 | 0.032 | 0.46 | 0.62 | 0.67 | 0.69 |
| NGC2419 | 11.198 | 0.009 | 10.727 | 0.009 | 10.473 | 0.009 | 10.371 | 0.010 | 0.01 | 0.01 | 0.01 | 0.01 |
| Pal3 | 15.389 | 0.046 | 14.824 | 0.036 | 14.585 | 0.033 | 14.304 | 0.043 | 0.01 | 0.03 | 0.04 | 0.04 |
| Pal4 | 15.284 | 0.052 | 14.636 | 0.058 | 14.293 | 0.083 | 14.074 | 0.107 | 0.00 | 0.00 | 0.00 | 0.00 |
| NGC4147 | 11.185 | 0.010 | 10.823 | 0.008 | 10.670 | 0.007 | 10.443 | 0.005 | 0.00 | 0.00 | 0.00 | 0.00 |
| NGC5024 | 8.518 | 0.003 | 8.122 | 0.004 | 7.991 | 0.003 | 7.676 | 0.003 | 0.00 | 0.00 | 0.00 | 0.00 |
| NGC5053 | 10.734 | 0.012 | 10.379 | 0.008 | 10.164 | 0.007 | 10.062 | 0.005 | 0.00 | 0.00 | 0.00 | 0.00 |
| NGC5272 | 7.071 | 0.002 | 6.712 | 0.002 | 6.555 | 0.001 | 6.135 | 0.002 | 0.00 | 0.00 | 0.00 | 0.00 |
| NGC5466 | 10.180 | 0.013 | 9.725 | 0.011 | 9.466 | 0.009 | 9.413 | 0.009 | 0.00 | 0.00 | 0.00 | 0.00 |
| Pal5 | 12.383 | 0.069 | 11.941 | 0.067 | 11.800 | 0.056 | 11.483 | 0.136 | 0.07 | 0.10 | 0.14 | 0.14 |
| Pal14 | 14.654 | 0.028 | 13.937 | 0.047 | 13.689 | 0.044 | 13.641 | 0.052 | 1.02 | 0.58 | 0.79 | 0.81 |
| NGC6205 | 6.903 | 0.005 | 6.667 | 0.003 | 6.397 | 0.004 | 6.076 | 0.002 | 0.00 | 0.00 | 0.00 | 0.00 |
| NGC6229 | 10.419 | 0.007 | 9.876 | 0.005 | 9.751 | 0.005 | 9.489 | 0.004 | 0.00 | 0.00 | 0.00 | 0.00 |
| Pal15 | 13.618 | 0.032 | 13.072 | 0.043 | 12.769 | 0.060 | 12.527 | 0.057 | 0.19 | 0.16 | 0.14 | 0.12 |
| NGC6535 | 10.274 | 0.030 | 9.901 | 0.029 | 9.773 | 0.033 | 9.470 | 0.040 | 0.11 | 0.08 | 0.06 | 0.06 |
| NGC6934 | 9.446 | 0.003 | 9.059 | 0.003 | 8.858 | 0.003 | 8.576 | 0.003 | 0.00 | 0.00 | 0.00 | 0.00 |
| NGC7006 | 11.320 | 0.012 | 10.817 | 0.012 | 10.554 | 0.012 | 10.436 | 0.012 | 0.02 | 0.02 | 0.02 | 0.02 |
| NGC7078 | 7.230 | 0.006 | 6.876 | 0.004 | 6.802 | 0.004 | 6.289 | 0.008 | 0.00 | 0.00 | 0.00 | 0.00 |
| NGC7089 | 7.298 | 0.003 | 6.854 | 0.004 | 6.758 | 0.004 | 6.407 | 0.002 | 0.00 | 0.00 | 0.00 | 0.00 |
| Pal13 | 15.736 | 0.060 | 15.392 | 0.050 | 15.270 | 0.048 | 15.147 | 0.049 | 0.00 | 0.00 | 0.00 | 0.00 |

the original Peng et al. (2006) hints at clouds or cirrus and this may be another possible reason for the difference. The RMS scatter of our photometry, compared with Peng et al. (2006), is 0.08 (0.07, 0.09) for g' (z' , $g' - z'$).

3.5 Photometric errors

Except for some poor clusters, the integrated magnitudes over the half-light radius have small random errors. The main contributions to the photometric error budget come from uncertainties in the photometric calibration and the centre determination (discussed above). For several clusters we have g' and z' data available from consecutive short and long exposures or from observations obtained during different nights. In this case the median magnitude of all observations is taken as the final magnitude in Table 2. In Fig. 4 we compare the magnitude differences between different observations (both performed on different nights or subsequent observations performed during the same night). The magnitudes in general compare well. However, there are some exceptions which will be treated later in this section.

First, we introduce some parameters that will be used to describe the details of these clusters. The standard way adopted in

this study to estimate the sky level was described in Section 3.2. We now refer to this sky determination as method A. To test the influence of the sky determination on the cluster magnitude, we estimate the sky contribution using a sky band, centred in the cluster centre, with an inner radius of 900 pixels and a width of 100 pixels. We refer to the latter as method B. The resulting magnitude difference between method A and method B is denoted as Δ_{AB}^* (with '*' indicating the filter). Tests on SDSS data did not result in significantly different sky estimates using methods A and B.

Another parameter used in the remainder of this section is $R_{GC/sky,*}$, which is the ratio of the sky-subtracted cluster flux to the sky flux (both measured within a half-light radius). Hence, when $R_{GC/sky,*} = 1$, the sky contribution is as strong as the cluster contribution to the flux within r_h . $R_{GC/sky,*} < 1$ when the sky contribution is higher than the pure (sky-subtracted) cluster contribution.

E 3 is a faint old cluster (12.8 Gyr, Marín-Franch et al. 2009) that may have been truncated by tidal forces (van den Bergh et al. 1980). Observations of 60 s were performed on both June 5 2004 and September 26 2005, with magnitude differences between both nights of 0.17 mag in g' and 0.02 mag in z' . It is suspicious that the magnitudes compare well for the z' filter, while they do

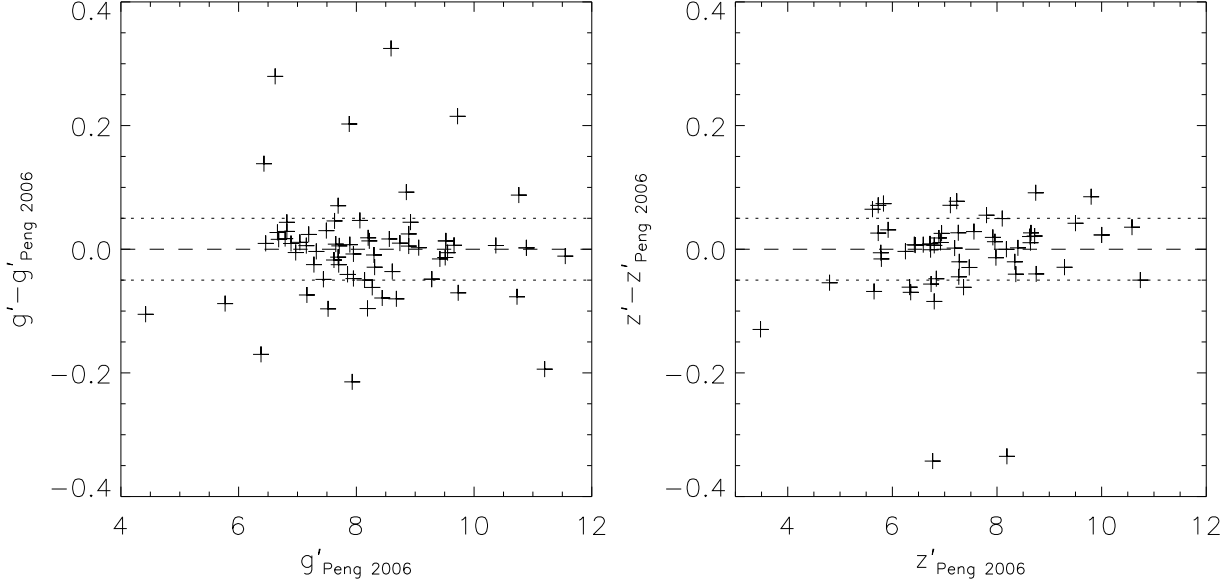


Figure 3. Comparison of the g' and z' magnitudes with the magnitudes obtained by Peng et al. (2006).

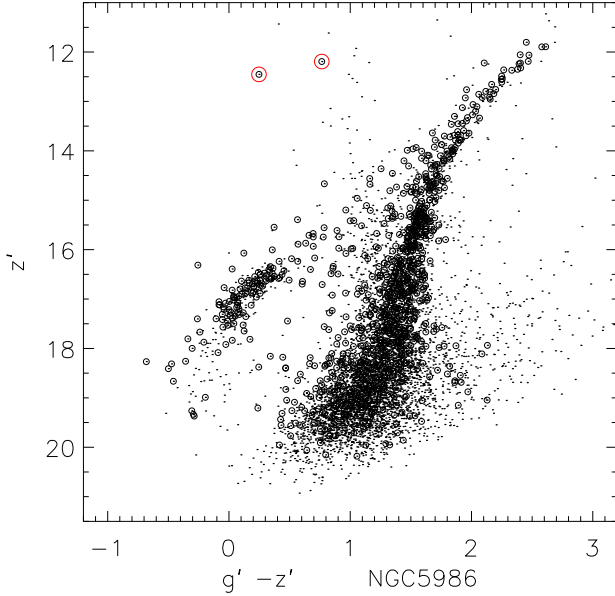


Figure 2. NGC 5986: open circles are stars within r_h , dots are stars from the entire field. The two bright isolated stars in the CMD (indicated with red circles) are selected as candidate outliers and were checked for proper motions. See text for more details.

not for the g' filter. In the latter filter, the average cluster surface brightness within a half-light radius is much lower than the brightness of the sky. Moreover, for the observations performed on June 5 2004, $R_{GC/Sky,g} = 0.18$, while on September 26 2005 $R_{GC/Sky,g} = 0.07$. This is a first indication the magnitude difference could be attributable to the sky uncertainty. Using method B (with the sky radius) instead of method A (with the four corners) results in an absolute g' magnitude difference $|\Delta_{AB}^{g'}| \sim 0.1$ mag, while the magnitude uncertainty is about 0.01 mag. This shows that the contribution of the sky uncertainty to the magnitude uncertainty is underestimated. Remark that the magnitude resulting using method B instead of method A was 0.1 mag brighter for the June 5

2004 observation ($\Delta_{AB}^{g'} \sim 0.1$ mag), while it was 0.1 mag fainter for the September 26 2005 observation ($\Delta_{AB}^{g'} \sim -0.1$ mag). For the z' filter, $R_{GC/Sky,z}$ is about 0.02 for both nights. The z' magnitudes are differing for both nights by $\Delta_{AB}^{z'} \sim -0.1$ mag when using a sky band instead of the 4 corner approach. Peng et al. (2006) did not include E 3 in their analysis because of the significant reddening ($E(B - V) \sim 0.3$, Harris 1996).

NGC6426, a high-reddening cluster with $E(B - V) \sim 0.36$, was observed on May 10, 2003 and on June 5 and 6, 2004. The g' -band magnitudes show significant variations between the nights: magnitudes obtained on May 10, 2003 were about 0.1 mag brighter than for the observations performed in June 2004. Taking the median of the observations performed on the different nights resulted in a g' magnitude consistent with all the June 2004 observations. The resulting z' magnitudes are all within 0.04 mag. Again, we want to pinpoint the influence of the sky determination on the magnitude discrepancies. The ratio $R_{GC/Sky,g}$ is about 0.6 for the observations performed on May 10 2003, while it is about 0.05 for the June 5 and 6 2004 observations. $\Delta_{AB}^{g'} \lesssim 0.02$ mag for the May 10 2003 observations, while these differences are as high as 0.34 mag (0.24 mag) for the June 5 (6, respectively) 2004 observations. For the 75 s and 410 s z' observations taken on May 10 2003, the ratio $R_{GC/Sky,z} \sim 0.1$, with $\Delta_{AB}^{z'} < 0.03$. For the 60 s observation performed on June 5 2004, $R_{GC/Sky,z} \sim 0.14$ and $\Delta_{AB}^{z'} \sim 0.24$, while for the 410 s observation taken on June 6 2004, $R_{GC/Sky,z} \sim 0.08$ and $\Delta_{AB}^{z'} \sim 0.15$. However, pure Poisson magnitude errors are smaller than 0.01. It is clear that some of the variation over the different nights can be attributed to the sky determination for this cluster.

Pal 3 is a low-reddening cluster ($E(B - V) \sim 0.04$) and was observed on June 5 and 6 2004. The magnitude difference in g' was about 0.19 mag (and 0.01 mag in z'). A bright star on the edge of the aperture complicates the determination of the magnitude. $R_{GC/Sky,g}$ amounts about 0.05 on both nights, while $R_{GC/Sky,z}$ varies between 0.002 and 0.02, so again the cluster is much fainter than the sky level. Using a sky band with MMM to estimate the sky value, results in g' (z') magnitude differences up to $\Delta_{AB}^{g'} \sim 1$

mag ($\Delta_{AB}^{z'} \sim 3.4$ mag, respectively). The sky values obtained with MMM in the corners (as described in Section 3.2) and the sky band are consistent within the large uncertainties. However, the photometric magnitude uncertainties given by the routine are large (up to $\sigma_{z'} \sim 0.23$), but not as large as the differences invoked by different sky estimation methods.

NGC 6584 was observed on May 10 2003 and June 5 2004. While g' magnitudes compare well for both nights, z' magnitudes show larger differences. For the z' observations performed on June 5, $R_{GC/Sky,z}$ is 0.86, while for the observations taken on May 10 it amounts to 0.60. $\Delta_{AB}^{z'} \sim 0.04$ mag for the June 2004 observation, while $\Delta_{AB}^{z'} \sim -0.02$ mag for the May 2003 observation. For this cluster, the sky determination seems not to be responsible for the magnitude offset. As a reference, we give some details on the g' observations as well. For the 37 s and 270 s observations performed on May 10 2003, $R_{GC/Sky,g} \sim 6$ and $\Delta_{AB}^{g'} < 0.01$ mag. For the observation obtained on June 5 2004, $R_{GC/Sky,g} \sim 0.53$ and the magnitude difference (using a sky band instead of the corners) is about $\Delta_{AB}^{g'} \sim 0.03$ mag.

Another cluster with a large difference between different observations is Terzan 7. This faint cluster was only observed on May 10 2003, but consecutive z' -band 79 s and 410 s observations showed magnitude variations about 0.1 mag. Because it is unlikely that, during a night that is considered photometric, the observing conditions change drastically in a ten minute timespan, this magnitude difference is surprising and deserves some special attention. This cluster, at a Galactic latitude of $b \sim -20^\circ$, is associated with the Sagittarius stream, hence located in a crowded field. This obviously complicates the sky determination: there is a difference of 0.7% between both sky determinations. However, as the surface brightness of the cluster is much lower than the sky level ($R_{GC/Sky,z} \sim 0.06$), this sky level difference results in a magnitude difference as stated above. This example again stresses the difficulty and importance of obtaining a reliable sky value. Nevertheless, the resulting magnitude errors are lower than 0.01 mag, hence the magnitude uncertainty is underestimated for this cluster. $|\Delta_{AB}^{z'}| \lesssim 0.01$ for both observations.

NGC 6121 is a bright high-reddening ($E(B - V) \sim 0.35$) cluster showing a z' magnitude difference of ~ 0.1 mag between the short 1 s exposure obtained on May 10 2003 ($z' \sim 4.37$) and the 11 s exposure performed on June 6 2004 ($z' \sim 4.47$). This cluster is located in a very crowded field ($l \sim 351^\circ$, $b \sim 16^\circ$), with a vast number of stars saturating the 60 s exposures. Nevertheless, for the short exposures, only few counts are collected to determine a reliable sky value. In the case of the 1 s exposure, the sky uncertainty obtained by MMM was larger than the sky value itself, with $R_{GC/Sky,z} \sim 1.2$ and $\Delta_{AB}^{z'} \sim -0.07$ mag, while for the 11 s exposure, $R_{GC/Sky,z} \sim 1.2$ and $\Delta_{AB}^{z'} \lesssim 0.01$ mag. On May 10 2003, the short 1 s exposure was followed by a long 410 s exposure, which could obviously not be used to determine the aperture magnitude of the cluster because of saturation issues. However, when using the long exposure to determine a more reliable sky value and then applying this sky value to the 1 s exposure, we obtain a magnitude 0.05 mag fainter than the value obtained above. Note that this value is fully consistent with the median value of the magnitudes obtained on both May 10 2003 and June 6 2004.

The scatter in Fig. 4 is larger than we would expect given the known error budget (photometric, centroiding, etc). We add a systematic contribution of 0.03 mag for g' and 0.0435 mag for z' , for the remainder of this analysis, to reduce the derived χ^2 to 1 and account for the additional photometric uncertainty. We cannot es-

Table 4. Median magnitude differences of clusters in common on different nights. Observations on September 26, 2005 had only few observations in common with other nights.

| Δ Nights | g' | z' |
|------------------|--------|--------|
| 5/10/03 – 6/5/04 | −0.004 | 0.015 |
| 5/10/03 – 6/6/04 | −0.008 | 0.007 |
| 6/5/04 – 6/6/04 | −0.002 | −0.002 |
| 6/5/04 – 9/26/05 | −0.004 | 0.001 |

timate this error for the other bands and we therefore adopt the z' error.

To demonstrate this error is not caused by a systematic photometric shift of certain nights, we present in Table 4 the median differences for clusters in common for the given nights.

3.6 Comparing CTIO and SDSS DR9

The CTIO and SDSS subsamples have 6 clusters in common for the g - and z -band and 4 GCs for r - and i -band. In Fig. 5 we compare the different magnitudes for the different filters. The included error bars are the combined errors of both magnitudes. The RMS for the magnitude difference between CTIO and SDSS data is 0.10, 0.18, 0.21 and 0.53 mag. for the g , r , i and z band respectively. NGC 7078 and NGC 7089 are the outliers in the i -band, Pal 3 and Pal 13 are the two z -band outliers. These objects contribute most to the high scatter.

Pal 3 has uncertain CTIO photometry, as was discussed in Section 3.5. It should be noted that the CTIO g' magnitude, based on the observations performed on June 6 2004, is consistent with the SDSS magnitude (within the large photometric uncertainty for this faint cluster). However, z' magnitudes based on CTIO observations on both June 5 and 6 2004 do not compare well with the SDSS magnitude for this filter. The issues regarding the sky determination for CTIO observations of this cluster were discussed in Section 3.5.

Pal 13 was only observed on September 26 2005 and has one of the highest specific frequencies of blue stragglers in any known GC (Clark et al. 2004). Based on the SDSS CMDs, one candidate outlier was identified. However, the star did not have proper motions, hence was not removed from the aperture photometry. This candidate outlier can not explain the $g - z$ colour difference between SDSS and CTIO: removing the star would have resulted in a $g - z$ colour correction of -0.04 . In Section 3.5 it became clear that a small variation in the CTIO sky determination can result in a large magnitude difference, especially for faint clusters which have a lower surface brightness than the sky itself. Motivated by the latter argument, we reinspected the CTIO sky determination for Pal 13. The $R_{GC/Sky,g} \sim 0.12$, while $R_{GC/Sky,z} \sim 0.01$, so the cluster flux contribution is much smaller than the sky contribution within a half-light radius. Using MMM on a sky ring of 900 to 1000 pixels (referred to as method B in Section 3.5) instead of the four corner approach (method A) results in magnitude differences of $\Delta_{AB}^{g'} \lesssim 0.003$ mag, while these rise to $\Delta_{AB}^{z'} \sim 0.35$ mag in the z' band. The large photometric uncertainties are reflected in the magnitude errors, though these are smaller than the difference invoked by using the different sky estimation methods.

Fig. 6 presents CMDs for NGC 6934 based on CTIO and SDSS data. It is clear that the RGB in the SDSS CMD suffers from saturation (it is known SDSS saturation starts at $r \sim 14$). Moreover, more blue stragglers are found in the CTIO CMD and the

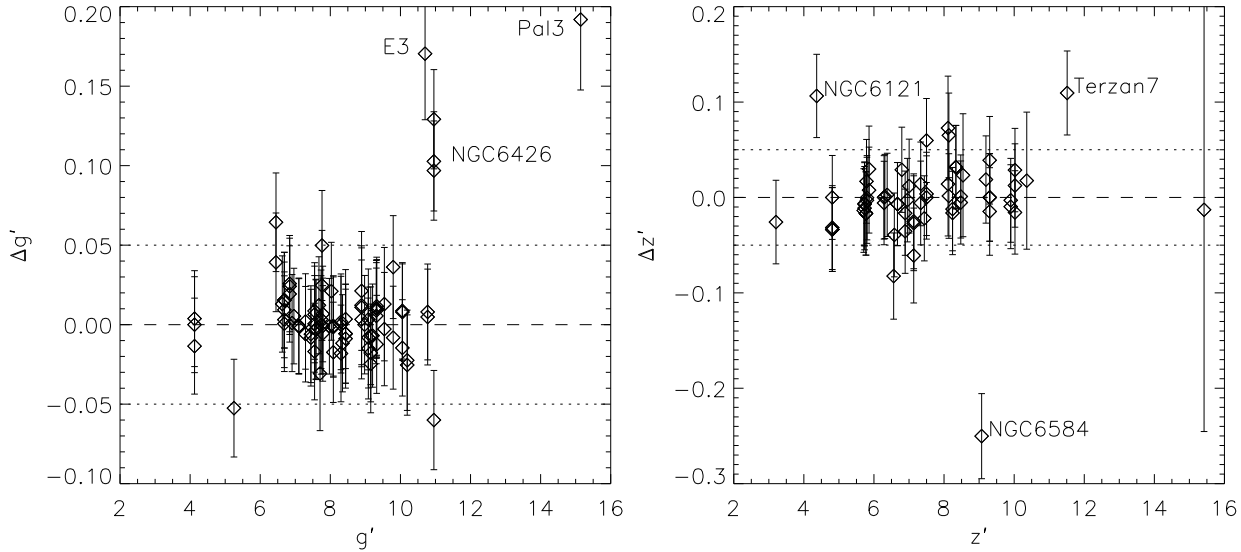


Figure 4. Comparison of g' and z' magnitudes, based on observations performed on different nights or performed subsequently during the same night). Error bars are including the systematic error.

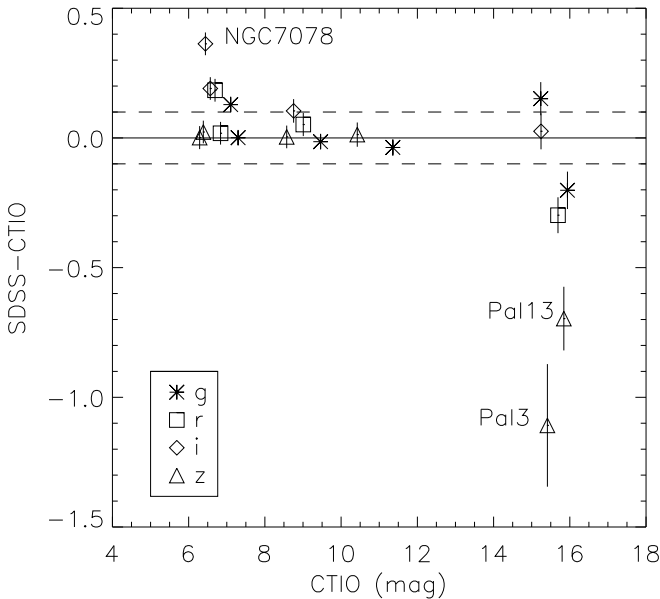


Figure 5. Comparison of magnitudes based on the CTIO observations and the SDSS DR9 survey. Error bars are the combined errors on both magnitudes.

blue HB is more extended than in the SDSS CMD. Further analysis of the CMDs will be presented in a subsequent paper. Nevertheless, when comparing the integrated magnitudes of NGC 6934, the agreement is excellent in grz while in the i -band magnitudes show a larger difference.

The SDSS data for NGC 7078 is also saturated for the RGB stars. Only for the z -band the difference between SDSS and CTIO data is smaller than 0.01 mag, for the other filters the differences are much larger. We observed this cluster with the CTIO 0.9m telescope on 3 different nights in the g' and z' filters. These 3 observations deviate less than 0.01 mag from each other in both filters. The cluster was also observed with the r' and i' filters but only for one night.

For the future work, we use the CTIO-based magnitudes whenever GCs have magnitudes from both subsamples, except for

Pal 3 and Pal 13, which are low-reddening clusters with very exceptional CTIO colours ($g' - z' \sim 0$), compared to $g' - z'$ colours of the other low-reddening clusters ranging between 0.4 and 1.4. We suspect issues with the sky determination for the CTIO data are causing the offsets with the SDSS data for these faint clusters.

4 SUMMARY

In the current study we presented integrated photometry for 96 Galactic GCs. We discuss a variety of issues, such as dealing with incomplete imaging (CCD cameras do not image the whole cluster), sky removal, calibration, the cleaning of contamination based on CMDs and proper motions and systematic errors. We obtained g' and z' magnitudes for about two-thirds of the Galactic GC system, making this the largest homogeneous optical sample based on the SDSS filter system. For about half of these clusters, we also present r' and i' photometry.

This work is the first of a series of papers, collected in the Galactic Globular Cluster Catalog (G2C2), exploiting this dataset of SDSS photometry. Future studies will deal with the colour-metallicity relations, the colour-magnitude diagrams, the spectral energy distributions, the structural parameters and the integrated spectroscopy.

ACKNOWLEDGMENTS

We thankfully acknowledge the anonymous referee for very useful and thought-provoking comments. We would like to thank Giovanni Carraro for fruitful discussions. JV acknowledges the support of ESO through a studentship. JV and MB acknowledge the support of the Fund for Scientific Research Flanders (FWO-Vlaanderen). AJ acknowledges support by the Chilean Ministry for the Economy, Development, and Tourism's Programa Iniciativa Científica Milenio through grant P07-021-F, awarded to The Milky Way Millennium Nucleus.

The authors are grateful to CTIO for the hospitality and the dedicated assistance during the numerous observing runs.

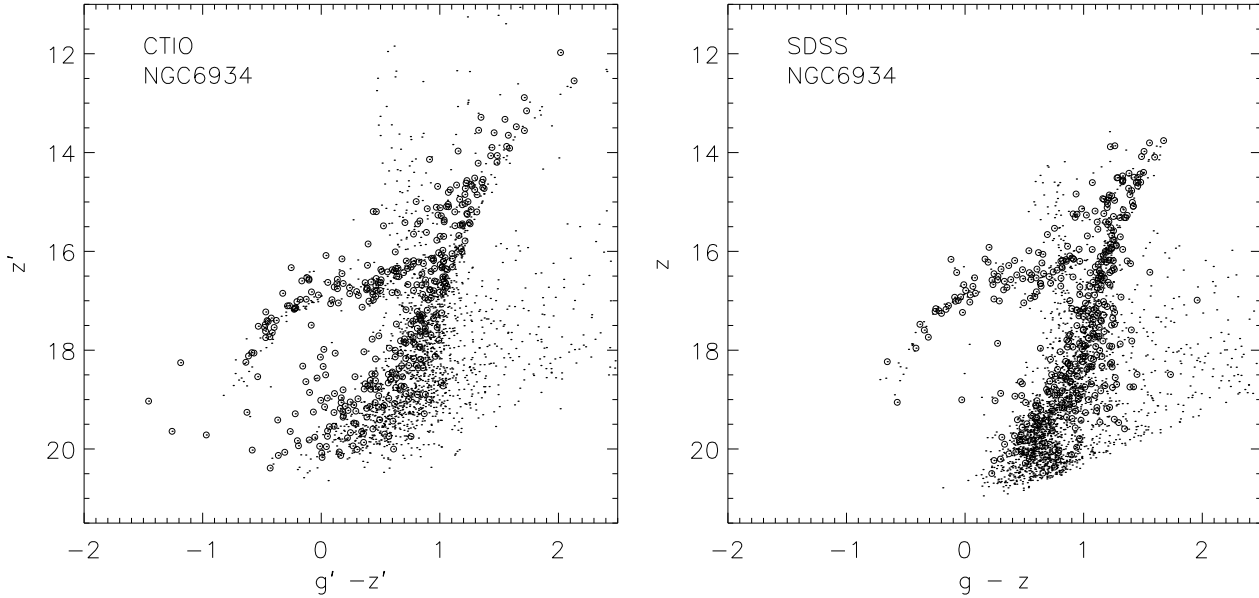


Figure 6. CMDs for NGC 6934 based on CTIO and SDSS data, using open circles for stars within r_h , dots for stars from the entire field. It is clear that saturation issues in the SDSS data sweep out the tip of the RGB. See text for more details.

This research has made use of NASA's Astrophysics Data System and the NED which is operated by the Jet Propulsion Laboratory, California Institute of Technology, under contract with the National Aeronautics and Space Administration.

This research made use of Montage, funded by the National Aeronautics and Space Administration's Earth Science Technology Office, Computation Technologies Project, under Cooperative Agreement Number NCC5-626 between NASA and the California Institute of Technology. Montage is maintained by the NASA/IPAC Infrared Science Archive.

For this part of the research, we have made extensive use of the European Virtual Observatory applications ALADIN (Bonnarel et al. 2000) and TOPCAT (Taylor 2005). The Virtual Observatory is a project designed to provide the astronomical community with the data access and the research tools necessary to enable the exploration of the digital, multi-wavelength universe resident in the astronomical data archives. We used the applications provided by astrometry.net³.

REFERENCES

- Ahn C. P., Alexandroff R., Allende Prieto C., et al., 2012, *ApJS*, 203, 21
- Alamo-Martínez K. A., Blakeslee J. P., Jee M. J., et al., 2013, *ArXiv e-prints*
- Alonso-García J., Mateo M., Sen B., et al., 2012, *AJ*, 143, 70
- Bellazzini M., 2007, *A&A*, 473, 171
- Bonnarel F., Fernique P., Bienaymé O., et al., 2000, *A&A Supl.*, 143, 33
- Brodie J. P., Strader J., 2006, *ARA&A*, 44, 193
- Cardelli J. A., Clayton G. C., Mathis J. S., 1989, *ApJ*, 345, 245
- Clark L. L., Sandquist E. L., Bolte M., 2004, *AJ*, 128, 3019
- Cohen J. G., Hsieh S., Metchev S., Djorgovski S. G., Malkan M., 2007, *AJ*, 133, 99
- Fukugita M., Ichikawa T., Gunn J. E., Doi M., Shimasaku K., Schneider D. P., 1996, *AJ*, 111, 1748
- Goldsbury R., Richer H. B., Anderson J., Dotter A., Sarajedini A., Woodley K., 2010, *AJ*, 140, 1830
- Harris W. E., 1991, *ARA&A*, 29, 543
- Harris W. E., 1996, *AJ*, 112, 1487
- Jordán A., Côté P., Blakeslee J. P., et al., 2005, *ApJ*, 634, 1002
- Marín-Franch A., Aparicio A., Piotto G., et al., 2009, *ApJ*, 694, 1498
- McDonald I., Zijlstra A. A., Rajoelimanana A. F., Johnson C. I., 2013, *MNRAS*, 429, L65
- McLaughlin D. E., van der Marel R. P., 2005, *ApJS*, 161, 304
- Monet D. G., Levine S. E., Canzian B., et al., 2003, *AJ*, 125, 984
- Patat F., Carraro G., 2001, *MNRAS*, 325, 1591
- Peacock M. B., Zepf S. E., Maccarone T. J., Kundu A., 2011, *ApJ*, 737, 5
- Peng E. W., Jordán A., Côté P., et al., 2006, *ApJ*, 639, 95
- Schlafly E. F., Finkbeiner D. P., 2011, *ApJ*, 737, 103
- Sinnott B., Hou A., Anderson R., Harris W. E., Woodley K. A., 2010, *AJ*, 140, 2101
- Smith J. A., Tucker D. L., Chen B., et al., 2000, in *American Astronomical Society Meeting Abstracts*, vol. 32 of *Bulletin of the American Astronomical Society*, 1424
- Smith J. A., Tucker D. L., Kent S., et al., 2002, *AJ*, 123, 2121
- Stetson P. B., 1987, *PASP*, 99, 191
- Stetson P. B., 1994, *PASP*, 106, 250
- Taylor M. B., 2005, in *Astronomical Data Analysis Software and Systems XIV*, edited by P. Shopbell, M. Britton, R. Ebert, vol. 347 of *Astronomical Society of the Pacific Conference Series*, 29
- Trager S. C., Djorgovski S., King I. R., 1993, in *Structure and Dynamics of Globular Clusters*, edited by S. G. Djorgovski, G. Meylan, vol. 50 of *Astronomical Society of the Pacific Conference Series*, 347
- Trager S. C., King I. R., Djorgovski S., 1995, *AJ*, 109, 218
- van den Bergh S., Demers S., Kunkel W. E., 1980, *ApJ*, 239, 112
- van Dokkum P. G., 2001, *PASP*, 113, 1420

³ <http://astrometry.net/>

- Vickers J. J., Grebel E. K., Huxor A. P., 2012, *AJ*, 143, 86
West M. J., Côté P., Marzke R. O., Jordán A., 2004, *Nature*, 427,
31
York D. G., Adelman J., Anderson Jr. J. E., et al., 2000, *AJ*, 120,
1579
Zacharias N., Monet D. G., Levine S. E., Urban S. E., Gaume R.,
Wycoff G. L., 2005, *VizieR Online Data Catalog*, 1297, 0

APPENDIX A: ONLINE TABLES

Table A1: GC $g'r'i'z'$ magnitudes and errors.

| ID | g' | $\sigma_{g'}$ | r' | $\sigma_{r'}$ | i' | $\sigma_{i'}$ | z' | $\sigma_{z'}$ | CMD $_{g'}$ | CMD $_{r'}$ | CMD $_{i'}$ | CMD $_{z'}$ |
|---------|--------|---------------|--------|---------------|--------|---------------|--------|---------------|-------------|-------------|-------------|-------------|
| NGC104 | 4.912 | 0.030 | ... | ... | ... | ... | 3.677 | 0.044 | 0.00 | ... | ... | 0.00 |
| NGC288 | 9.080 | 0.032 | 8.600 | 0.045 | 8.295 | 0.044 | 8.139 | 0.044 | 0.00 | 0.00 | 0.00 | 0.00 |
| NGC362 | 7.471 | 0.030 | 6.925 | 0.043 | 6.618 | 0.043 | 6.419 | 0.043 | 0.01 | 0.02 | 0.02 | 0.03 |
| NGC1261 | 9.474 | 0.031 | 8.995 | 0.045 | 8.744 | 0.045 | 8.582 | 0.045 | 0.03 | 0.05 | 0.06 | 0.06 |
| AM1 | 15.958 | 0.035 | 15.582 | 0.046 | 15.219 | 0.047 | 15.159 | 0.056 | 0.07 | 0.13 | 0.14 | 0.16 |
| NGC1851 | 8.280 | 0.031 | 7.703 | 0.044 | 7.413 | 0.044 | 7.194 | 0.044 | 0.03 | 0.04 | 0.05 | 0.05 |
| NGC1904 | 9.006 | 0.030 | 8.570 | 0.044 | 8.351 | 0.044 | 8.178 | 0.044 | 0.02 | 0.04 | 0.05 | 0.05 |
| NGC2298 | 9.650 | 0.039 | 9.287 | 0.050 | 9.036 | 0.052 | 8.865 | 0.054 | 0.06 | 0.10 | 0.10 | 0.10 |
| NGC2808 | 6.695 | 0.030 | 6.194 | 0.044 | 5.916 | 0.044 | 5.725 | 0.044 | 0.00 | 0.00 | 0.00 | 0.00 |
| E3 | 10.787 | 0.041 | ... | ... | ... | ... | 10.368 | 0.072 | 0.00 | ... | ... | 0.00 |
| Pal3 | 15.238 | 0.044 | ... | ... | ... | ... | 15.412 | 0.232 | 0.00 | ... | ... | 0.00 |
| NGC3201 | 7.006 | 0.033 | ... | ... | ... | ... | ... | ... | 0.01 | ... | ... | 0.00 |
| NGC4372 | 6.489 | 0.031 | ... | ... | ... | ... | 5.796 | 0.044 | 0.00 | ... | ... | 0.00 |
| Rup106 | 11.981 | 0.031 | ... | ... | ... | ... | 11.204 | 0.168 | 0.59 | ... | ... | 0.69 |
| NGC4590 | 8.903 | 0.037 | ... | ... | ... | ... | 8.127 | 0.054 | 0.00 | ... | ... | 0.00 |
| NGC4833 | 7.034 | 0.034 | ... | ... | ... | ... | ... | ... | 0.03 | ... | ... | 0.02 |
| NGC5139 | 4.131 | 0.030 | ... | ... | ... | ... | 3.198 | 0.044 | 0.01 | ... | ... | 0.01 |
| NGC5286 | 7.551 | 0.030 | ... | ... | ... | ... | 6.664 | 0.044 | 0.00 | ... | ... | 0.00 |
| NGC5634 | 10.060 | 0.030 | ... | ... | ... | ... | 9.205 | 0.046 | 0.00 | ... | ... | 0.00 |
| NGC5694 | 10.781 | 0.030 | ... | ... | ... | ... | 9.899 | 0.044 | 0.00 | ... | ... | 0.00 |
| IC4499 | 10.256 | 0.032 | 9.820 | 0.044 | 9.520 | 0.044 | 9.372 | 0.044 | 0.18 | 0.24 | 0.23 | 0.22 |
| NGC5824 | 9.321 | 0.030 | 8.876 | 0.043 | 8.648 | 0.043 | 8.477 | 0.043 | 0.00 | 0.00 | 0.00 | 0.00 |
| NGC5897 | 9.171 | 0.031 | 8.835 | 0.044 | 8.542 | 0.044 | 8.414 | 0.044 | 0.03 | 0.04 | 0.04 | 0.04 |
| NGC5904 | 6.861 | 0.030 | ... | ... | ... | ... | 5.867 | 0.045 | 0.00 | ... | ... | 0.00 |
| NGC5927 | 7.785 | 0.030 | 7.184 | 0.043 | 6.816 | 0.044 | 6.521 | 0.045 | 0.00 | 0.00 | 0.00 | 0.00 |
| NGC5946 | 8.340 | 0.031 | 7.889 | 0.044 | 7.645 | 0.045 | 7.477 | 0.045 | 0.30 | 0.14 | 0.08 | 0.05 |
| NGC5986 | 7.794 | 0.031 | 7.349 | 0.045 | 7.072 | 0.044 | 6.894 | 0.044 | 0.06 | 0.03 | 0.02 | 0.02 |
| NGC6093 | 7.924 | 0.030 | 7.417 | 0.044 | 7.148 | 0.044 | 6.939 | 0.044 | 0.00 | 0.00 | 0.00 | 0.00 |
| NGC6121 | 5.251 | 0.031 | ... | ... | ... | ... | 4.435 | 0.044 | 0.03 | ... | ... | 0.02 |
| NGC6101 | 10.171 | 0.032 | 9.736 | 0.045 | 9.460 | 0.044 | 9.301 | 0.046 | 0.00 | 0.00 | 0.00 | 0.00 |
| NGC6144 | 7.876 | 0.031 | 7.811 | 0.044 | 7.689 | 0.044 | 7.602 | 0.044 | 0.19 | 0.13 | 0.09 | 0.07 |
| NGC6139 | 7.375 | 0.030 | ... | ... | ... | ... | 6.623 | 0.044 | 0.00 | ... | ... | 0.00 |
| NGC6171 | 8.084 | 0.032 | ... | ... | ... | ... | 7.109 | 0.050 | 0.00 | ... | ... | 0.00 |
| NGC6218 | 7.691 | 0.036 | ... | ... | ... | ... | 6.653 | 0.053 | 0.00 | ... | ... | 0.00 |
| NGC6235 | 9.542 | 0.036 | ... | ... | ... | ... | 8.552 | 0.064 | 0.00 | ... | ... | 0.00 |
| NGC6254 | 6.842 | 0.031 | ... | ... | ... | ... | ... | ... | ... | ... | ... | ... |
| NGC6273 | 6.909 | 0.031 | ... | ... | ... | ... | 5.801 | 0.044 | 0.00 | ... | ... | 0.00 |
| NGC6284 | 9.247 | 0.030 | ... | ... | ... | ... | 8.145 | 0.044 | 0.00 | ... | ... | 0.00 |
| NGC6287 | 8.121 | 0.030 | 7.811 | 0.046 | 7.580 | 0.045 | 7.426 | 0.044 | 0.00 | 0.00 | 0.00 | 0.00 |
| NGC6293 | 7.440 | 0.030 | ... | ... | ... | ... | 6.999 | 0.044 | 0.00 | ... | ... | 0.05 |
| NGC6304 | 7.677 | 0.030 | ... | ... | ... | ... | 6.313 | 0.044 | 0.00 | ... | ... | 0.00 |
| NGC6316 | 8.131 | 0.030 | ... | ... | ... | ... | 7.090 | 0.043 | 0.00 | ... | ... | 0.00 |
| NGC6333 | 7.467 | 0.032 | ... | ... | ... | ... | 6.676 | 0.044 | 0.00 | ... | ... | 0.00 |
| NGC6342 | 9.327 | 0.031 | ... | ... | ... | ... | 8.231 | 0.044 | 0.00 | ... | ... | 0.00 |
| NGC6356 | 8.499 | 0.031 | ... | ... | ... | ... | 7.231 | 0.048 | 0.01 | ... | ... | 0.03 |
| NGC6355 | 7.413 | 0.039 | ... | ... | ... | ... | 6.908 | 0.049 | 0.00 | ... | ... | 0.00 |
| NGC6352 | 7.788 | 0.035 | ... | ... | ... | ... | 6.562 | 0.044 | 0.00 | ... | ... | 0.00 |
| IC1257 | ... | ... | 10.927 | 0.045 | 10.719 | 0.046 | ... | ... | ... | 0.12 | 0.13 | ... |
| NGC6366 | 7.736 | 0.031 | ... | ... | ... | ... | 6.769 | 0.044 | 0.23 | ... | ... | 0.10 |
| NGC6362 | 8.429 | 0.031 | ... | ... | ... | ... | 7.334 | 0.044 | 0.00 | ... | ... | 0.00 |
| NGC6388 | 6.962 | 0.030 | ... | ... | ... | ... | 5.754 | 0.044 | 0.00 | ... | ... | 0.00 |
| NGC6402 | 7.503 | 0.030 | ... | ... | ... | ... | 6.203 | 0.044 | 0.00 | ... | ... | 0.00 |
| NGC6401 | 7.373 | 0.036 | ... | ... | ... | ... | ... | ... | ... | ... | ... | ... |
| NGC6397 | ... | ... | ... | ... | ... | ... | 5.450 | 0.044 | 0.00 | ... | ... | 0.00 |
| NGC6426 | 11.051 | 0.031 | ... | ... | ... | ... | 10.030 | 0.044 | 0.00 | ... | ... | 0.00 |
| NGC6440 | 7.504 | 0.030 | ... | ... | ... | ... | 6.080 | 0.044 | 0.00 | ... | ... | 0.00 |
| NGC6441 | 6.635 | 0.030 | ... | ... | ... | ... | 5.700 | 0.044 | 0.00 | ... | ... | 0.00 |

Continued on next page

Table A1 – continued from previous page

| ID | g' | $\sigma_{g'}$ | r' | $\sigma_{r'}$ | i' | $\sigma_{i'}$ | z' | $\sigma_{z'}$ | CMD $_{g'}$ | CMD $_{r'}$ | CMD $_{i'}$ | CMD $_{z'}$ |
|---------|--------|---------------|--------|---------------|--------|---------------|--------|---------------|-------------|-------------|-------------|-------------|
| NGC6453 | 9.016 | 0.031 | 8.381 | 0.044 | ... | ... | ... | ... | ... | ... | ... | ... |
| NGC6496 | 10.095 | 0.055 | ... | ... | ... | ... | ... | ... | 0.49 | ... | ... | 0.55 |
| NGC6517 | 8.298 | 0.030 | 7.918 | 0.043 | 7.613 | 0.044 | 7.411 | 0.044 | 0.00 | 0.00 | 0.00 | 0.00 |
| NGC6539 | 7.740 | 0.036 | 7.148 | 0.044 | 6.738 | 0.044 | 6.457 | 0.045 | 0.22 | 0.14 | 0.12 | 0.11 |
| NGC6544 | 3.941 | 0.033 | 4.341 | 0.045 | ... | ... | ... | ... | ... | ... | ... | ... |
| NGC6541 | 7.262 | 0.031 | ... | ... | ... | ... | ... | ... | 0.00 | ... | ... | 0.01 |
| NGC6553 | 5.254 | 0.030 | 5.145 | 0.044 | 4.966 | 0.044 | 4.822 | 0.044 | 0.19 | 0.09 | 0.06 | 0.04 |
| NGC6558 | 7.751 | 0.035 | 7.238 | 0.045 | 6.976 | 0.045 | 6.866 | 0.044 | 0.00 | 0.00 | 0.00 | 0.00 |
| IC1276 | 6.814 | 0.037 | 6.427 | 0.044 | 6.148 | 0.044 | 6.016 | 0.045 | 0.19 | 0.14 | 0.18 | 0.22 |
| NGC6569 | 8.801 | 0.031 | 8.048 | 0.044 | 7.605 | 0.044 | 7.278 | 0.044 | 0.05 | 0.04 | 0.03 | 0.04 |
| NGC6584 | 9.793 | 0.032 | 9.279 | 0.051 | 9.017 | 0.048 | 8.947 | 0.045 | 0.00 | 0.00 | 0.00 | 0.00 |
| NGC6624 | 8.341 | 0.031 | 7.696 | 0.044 | 7.285 | 0.046 | 7.009 | 0.049 | 0.00 | 0.00 | 0.00 | 0.00 |
| NGC6626 | 6.180 | 0.030 | 5.706 | 0.044 | 5.424 | 0.044 | ... | ... | ... | ... | ... | ... |
| NGC6638 | 8.977 | 0.031 | 8.351 | 0.044 | 8.033 | 0.044 | 7.849 | 0.044 | 0.00 | 0.00 | 0.00 | 0.00 |
| NGC6637 | 8.295 | 0.064 | 7.693 | 0.048 | 7.306 | 0.049 | ... | ... | 0.00 | 0.00 | 0.00 | 0.00 |
| NGC6642 | 9.309 | 0.032 | ... | ... | ... | ... | 8.152 | 0.046 | 0.11 | ... | ... | 0.12 |
| NGC6652 | 9.818 | 0.031 | ... | ... | ... | ... | 8.737 | 0.046 | 0.00 | ... | ... | 0.00 |
| Pal8 | 10.569 | 0.031 | ... | ... | ... | ... | 9.349 | 0.045 | 0.01 | ... | ... | 0.11 |
| NGC6681 | 8.859 | 0.030 | ... | ... | ... | ... | ... | ... | 0.00 | ... | ... | 0.00 |
| NGC6712 | 7.955 | 0.030 | ... | ... | ... | ... | ... | ... | 0.00 | ... | ... | 0.00 |
| NGC6715 | 7.973 | 0.030 | ... | ... | ... | ... | 6.946 | 0.043 | 0.00 | ... | ... | 0.00 |
| NGC6723 | 7.585 | 0.031 | ... | ... | ... | ... | 6.810 | 0.045 | 0.00 | ... | ... | 0.00 |
| NGC6749 | 6.735 | 0.045 | ... | ... | ... | ... | 6.341 | 0.044 | 0.41 | ... | ... | 0.05 |
| NGC6760 | 8.304 | 0.030 | ... | ... | ... | ... | 6.522 | 0.044 | 0.00 | ... | ... | 0.00 |
| NGC6779 | 8.613 | 0.030 | 8.138 | 0.044 | 7.879 | 0.044 | 7.748 | 0.044 | 0.00 | 0.00 | 0.00 | 0.00 |
| Terzan7 | 12.469 | 0.031 | ... | ... | ... | ... | 11.567 | 0.044 | 0.00 | ... | ... | 0.00 |
| Pal10 | 7.862 | 0.039 | 7.498 | 0.050 | 7.328 | 0.056 | 7.216 | 0.047 | 1.33 | 0.62 | 0.39 | 0.33 |
| Pal11 | 11.439 | 0.034 | ... | ... | ... | ... | 10.413 | 0.048 | 0.00 | ... | ... | 0.00 |
| NGC6838 | 7.973 | 0.039 | ... | ... | ... | ... | ... | ... | 0.00 | ... | ... | 0.00 |
| NGC6864 | 9.167 | 0.030 | 8.608 | 0.044 | 8.320 | 0.044 | 8.099 | 0.044 | 0.00 | 0.00 | 0.00 | 0.00 |
| NGC6934 | 9.460 | 0.030 | 9.007 | 0.045 | 8.754 | 0.045 | 8.572 | 0.044 | 0.00 | 0.00 | 0.00 | 0.00 |
| NGC6981 | 10.132 | 0.031 | 9.666 | 0.045 | 9.391 | 0.045 | 9.213 | 0.046 | 0.00 | 0.00 | 0.00 | 0.00 |
| NGC7006 | 11.357 | 0.030 | ... | ... | ... | ... | 10.423 | 0.045 | 0.03 | ... | ... | 0.02 |
| NGC7078 | 7.101 | 0.030 | 6.692 | 0.044 | 6.439 | 0.044 | 6.288 | 0.044 | 0.00 | 0.00 | 0.00 | 0.00 |
| NGC7089 | 7.297 | 0.030 | 6.836 | 0.044 | 6.567 | 0.044 | 6.384 | 0.044 | 0.00 | 0.01 | 0.00 | 0.00 |
| NGC7099 | 8.306 | 0.030 | ... | ... | ... | ... | 7.501 | 0.044 | 0.00 | ... | ... | 0.00 |
| Pal12 | 12.489 | 0.030 | 11.826 | 0.043 | 11.482 | 0.044 | 11.345 | 0.045 | 1.38 | 1.24 | 1.15 | 1.06 |
| Pal13 | 15.938 | 0.040 | 15.690 | 0.048 | 15.244 | 0.051 | 15.843 | 0.112 | 0.00 | 0.00 | 0.00 | 0.00 |
| NGC7492 | 12.197 | 0.038 | 11.824 | 0.045 | 11.570 | 0.044 | 11.560 | 0.046 | 0.00 | 0.00 | 0.00 | 0.00 |